TABLE II. Diagrams of symmetric networks with $N = 6$, 7, and 8 nodes.

$N = 6$	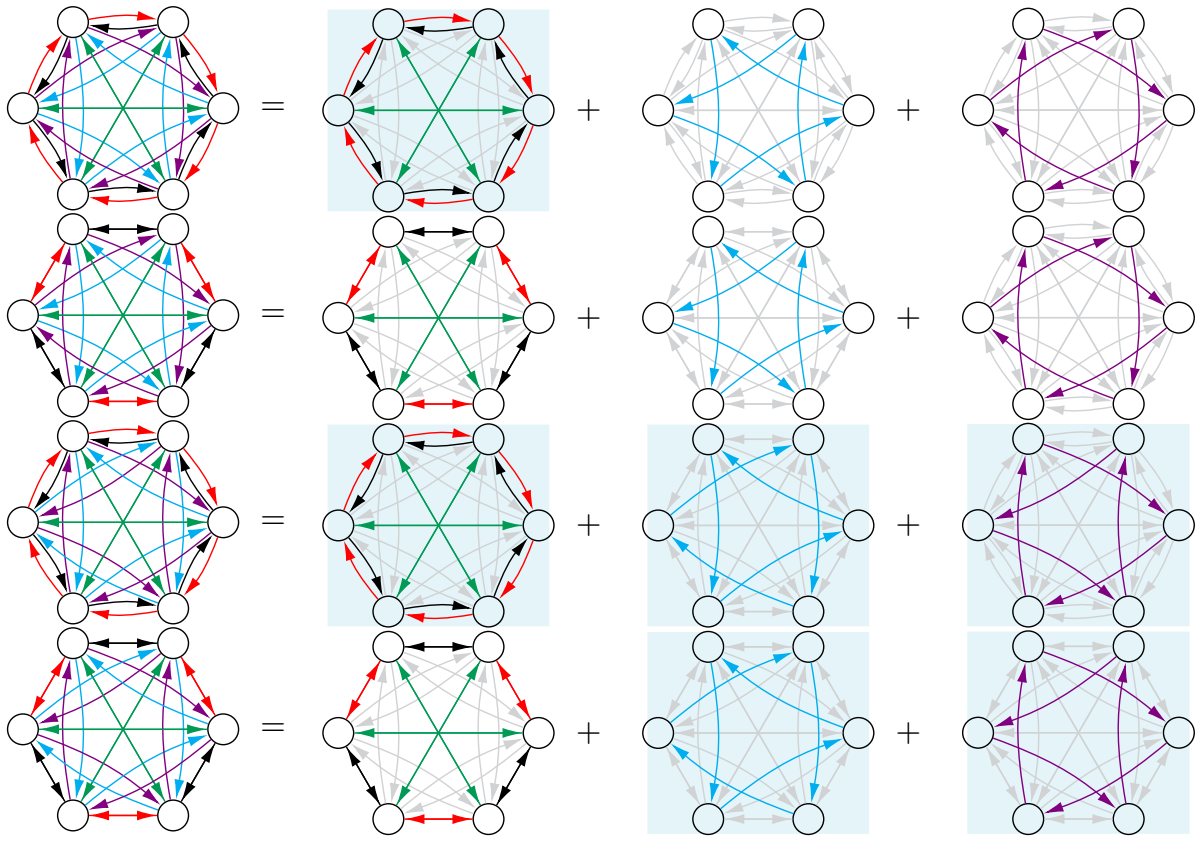
$N = 7$	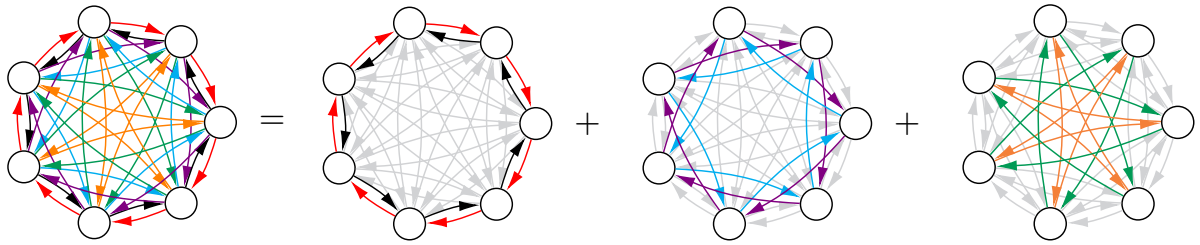
$N = 8$	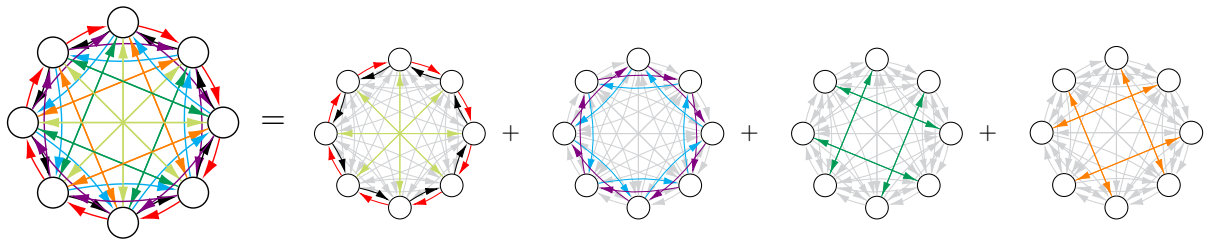 and 11 others

VII. DISCUSSION

Given a symmetric network of identical oscillators, it is instructive to compare our results above in which the symmetry is broken by making the oscillators nonidentical with the alternative scenario in which the symmetry is broken by making the network structure asymmetric. For directed unweighted networks of diffusively-coupled identical oscillators, it can be shown that: 1) with the exception of the complete graphs, all topologies that optimize synchronizability (i.e., those with $\sigma = 0$) are asymmetric; 2) any network topology that can be spanned from a node (i.e., $\min_{i\geq 2} \mathrm{Re}(\lambda_i) > 0$) embeds optimally syn-

chronizable subnetworks generated by deleting a subset of links [8, 28]. For example, a synchronous state that is not stable for a directed ring network may become stable for a directed chain formed by removing a link. More generally, introducing structural heterogeneity (breaking the symmetry of the network) can stabilize otherwise unstable homogeneous (symmetric) states.

Finally, we note that the defining characteristic of *AISync* considered here—that preserving the symmetry of a stable state requires breaking the symmetry of the system—can bear analogs in oscillator networks whose structure is not necessarily symmetric. Such a network can always be partitioned into symmetric subnetwork clusters (structurally equivalent subsets of nodes) that are candidates for cluster synchronization [16, 29, 30]. Synchronization of one of these clusters plays the role of complete synchronization in a symmetric network, which opens the possibility of exploiting *AISync* to tune cluster synchronization patterns through oscillator heterogeneity in arbitrary complex networks. We hope that our findings, and future theoretical and experimental studies they will stimulate, will significantly advance understanding of the interplay between symmetry and network dynamics.

ACKNOWLEDGMENTS

The authors thank Thomas Wytock and Young Sul Cho for insightful discussions. This work was supported by ARO Grant No. W911NF-15-1-0272.

Appendix A: Definition of Cayley graphs

Given a generating set S of a finite group G, the Cayley graph associated with S and G is defined as the network in which a node represents an element of G and a directed link from one node $g \in G$ to another $g' \in G$ represents the composition of some element $s \in S$ with g that gives g' (i.e., $gs = g'$). While such a network is generally directed, it will be undirected if the inverse of every element of S belongs to S. Choosing S to be a generating set guarantees that the resulting network is (strongly) connected. A generalization to multiple link types can be obtained if we assign different elements of S to different link types.

Appendix B: Details on multilayer models

Since Eq. (2) defines a subclass of systems governed by Eq. (1), it can always be written in the form of Eq. (1) for a given network structure specified by $A^{(\alpha)}$. This can be seen by stacking the m-dimensional vectors in Eq. (2) and defining appropriate functions as follows:

$$\boldsymbol{X}_i := \begin{pmatrix} \boldsymbol{x}_1^{(i)} \\ \vdots \\ \boldsymbol{x}_L^{(i)} \end{pmatrix}, \quad \boldsymbol{F}_i := \begin{pmatrix} \boldsymbol{F}_1^{(i)} \\ \vdots \\ \boldsymbol{F}_L^{(i)} \end{pmatrix}, \quad \boldsymbol{H}^{(\alpha)} := \begin{pmatrix} \boldsymbol{H}_1^{(\alpha)} \\ \vdots \\ \boldsymbol{H}_L^{(\alpha)} \end{pmatrix}, \tag{B1}$$

$$\boldsymbol{F}_\ell^{(i)}(\boldsymbol{X}_i) := \boldsymbol{f}(\boldsymbol{x}_\ell^{(i)}) + \sum_{\ell'=1}^{L} \widetilde{A}_{\ell\ell'}^{(ii)}[\boldsymbol{h}(\boldsymbol{x}_{\ell'}^{(i)}) - \boldsymbol{h}(\boldsymbol{x}_\ell^{(i)})], \tag{B2}$$

$$\boldsymbol{H}_\ell^{(\alpha)}(\boldsymbol{X}_i, \boldsymbol{X}_{i'}) := \sum_{\ell'=1}^{L} B_{\ell\ell'}^{(\alpha)}[\boldsymbol{h}(\boldsymbol{x}_{\ell'}^{(i')}) - \boldsymbol{h}(\boldsymbol{x}_\ell^{(i)})], \tag{B3}$$

where $B_{\ell\ell'}^{(\alpha)}$ is defined to be the value of $\widetilde{A}_{\ell\ell'}^{(ii')}$ when node i' is connected to node i by a link of type α. Note that these node-to-node interactions are not necessarily diffusive, since we can have $\boldsymbol{H}^{(\alpha)}(\boldsymbol{X}_i, \boldsymbol{X}_{i'}) \neq \boldsymbol{0}$ even for $\boldsymbol{X}_i = \boldsymbol{X}_{i'}$, if $\boldsymbol{x}_\ell^{(i)} \neq \boldsymbol{x}_{\ell'}^{(i')}$ for some $\ell \neq \ell'$ [which in particular means that the coupling term cannot be written in the form $\boldsymbol{H}^{(\alpha)}(\boldsymbol{X}_i, \boldsymbol{X}_{i'}) = \widetilde{\boldsymbol{H}}^{(\alpha)}(\boldsymbol{X}_{i'}) - \widetilde{\boldsymbol{H}}^{(\alpha)}(\boldsymbol{X}_i)$]. For example, even when nodes 1 and 4 are synchronized in the network of Fig. 1, i.e., $\boldsymbol{X}_1 = \boldsymbol{X}_4 = (\boldsymbol{s}_1(t), \boldsymbol{s}_2(t))^T$, the coupling term corresponding to the link of type $\alpha = 3$ between them is in general not identically zero:

$$\boldsymbol{H}^{(3)}(\boldsymbol{X}_1, \boldsymbol{X}_4) = \begin{pmatrix} \boldsymbol{h}(\boldsymbol{s}_2) - \boldsymbol{h}(\boldsymbol{s}_1) \\ 0 \end{pmatrix} \not\equiv \boldsymbol{0}. \tag{B4}$$

However, since we assume identical dynamics for subnodes and diffusive coupling between subnodes, a synchronous state of Eq. (2) given by $\boldsymbol{x}_\ell^{(i)}(t) = \boldsymbol{s}(t)$, $\forall i, \ell$ with $\dot{\boldsymbol{s}} = \boldsymbol{f}(\boldsymbol{s})$ is guaranteed to exist even if $F^{(i)}$'s are heterogeneous. This corresponds to a global synchronous state of Eq. (1) defined by $\boldsymbol{X}_i = \boldsymbol{S} := (\boldsymbol{s}, \ldots, \boldsymbol{s})^T$, $\forall i$, which can be verified by noting that $\boldsymbol{H}^{(\alpha)}(\boldsymbol{S}, \boldsymbol{S}) = \boldsymbol{0}$ and $\boldsymbol{F}_\ell^{(i)}(\boldsymbol{S}) := \boldsymbol{f}(\boldsymbol{s})$, $\forall i, \ell$.

Appendix C: Details on MSF analysis

Equation (2) can be rewritten as a monolayer network by defining a single index for all the $n := LN$ subnodes, in which node i has subnodes $j = k_{i1}, \ldots, k_{iL}$ with $k_{i\ell} := (i-1)L + \ell$. This leads to the standard form for a (monolayer) diffusively coupled network of oscillators:

$$\dot{\boldsymbol{x}}_j = \boldsymbol{f}(\boldsymbol{x}_j) + \sum_{j'=1}^{n} \widetilde{A}_{jj'}[\boldsymbol{h}(\boldsymbol{x}_{j'}) - \boldsymbol{h}(\boldsymbol{x}_j)], \tag{C1}$$

where $\boldsymbol{x}_j = \boldsymbol{x}_\ell^{(i)}$ and $\widetilde{A}_{jj'} := \widetilde{A}_{\ell\ell'}^{(ii')}$ for $j = k_{i\ell}$ and $j' = k_{i'\ell'}$. In the monolayer adjacency matrix $\widetilde{A} = (\widetilde{A}_{jj'})$, the matrix $B^{(\alpha)} = (B_{\ell\ell'}^{(\alpha)})$ appears as multiple off-diagonal blocks of size L, and the arrangement of those blocks within $\widetilde{A}$ matches with the structure of the corresponding

adjacency matrix $A^{(\alpha)}$, reflecting the topology of node-to-node interactions through links of type α [see Fig. 1(d) for an example]. This equation allows application of the MSF analysis [25] because subnodes and sublinks (and the associated coupling functions) are identical. The stability function $\psi(\lambda)$ is defined as the maximum Lyapunov exponent of the reduced variational equation,

$$\dot{\boldsymbol{\xi}} = [D\boldsymbol{f}(\boldsymbol{s}) - \lambda D\boldsymbol{h}(\boldsymbol{s})]\boldsymbol{\xi}, \tag{C2}$$

where $\boldsymbol{\xi}$ is an m-dimensional perturbation vector, $D\boldsymbol{f}(\boldsymbol{s})$ and $D\boldsymbol{h}(\boldsymbol{s})$ are the Jacobian of $\boldsymbol{f}$ and $\boldsymbol{h}$, respectively, at the synchronous state, $\boldsymbol{x}_j = \boldsymbol{s}(t)$, $\forall j$, and λ is a complex-valued parameter.

Appendix D: Verifying the *AISync* conditions

Here we describe our scheme for verifying *AISync* conditions (C1) and (C2) given a symmetric network structure (adjacency matrices $A^{(\alpha)}$), external sublink configurations (matrices $B^{(\alpha)}$), a set $\mathcal{F}$ of possible internal sublink configurations (from which matrices $F^{(i)}$ are chosen), isolated subnode dynamics $\boldsymbol{f}$, and sublink coupling function $\boldsymbol{h}$. We first obtain the stability function $\psi(\lambda)$:

1. Compute a trajectory $\boldsymbol{s}(t)$ of an isolated subnode by integrating $\dot{\boldsymbol{s}} = \boldsymbol{f}(\boldsymbol{s})$, which determines the synchronous state, $\boldsymbol{x}_\ell^{(i)}(t) = \boldsymbol{s}(t)$, $\forall i, \ell$.

2. Integrate Eq. (C2) and calculate its maximum Lyapunov exponent (MLE), which defines $\psi(\lambda)$ for a range of λ in the complex plane.

Note that $\psi(\lambda)$ depends only on $\boldsymbol{f}$, $\boldsymbol{h}$, and $\boldsymbol{s}(t)$. For a given symmetric network structure and external sublink configurations, we can compute the stability Ψ of the synchronous state for any combination of $F^{(i)} \in \mathcal{F}$ by calculating and substituting the Laplacian eigenvalues λ_j into the formula $\Psi = \max_{2\le j\le n} \psi(\lambda_j)$. To establish the *AISync* property, we verify the following conditions:

- (C1)′: For each matrix $F \in \mathcal{F}$, set $F^{(1)} = \cdots = F^{(N)} = F$ (leading to a homogeneous system) and verify $\Psi > 0$.

- (C2)′: Identify a combination of (heterogeneous) $F^{(i)} \in \mathcal{F}$ for which $\Psi < 0$ (e.g., by checking exhaustively or by using a numerical optimization algorithm to minimize Ψ over $F^{(i)}$).

The verification of condition (C1)′ provides strong support for (C1), since the only other possibility for a stable synchronization of all nodes is a state of the form $\boldsymbol{x}_\ell^{(i)} = \boldsymbol{s}_\ell(t)$, $\forall i, \ell$, with at least one $\boldsymbol{s}_\ell(t)$ different from the others (which we find does not exist in many cases, such as the examples in Fig. 3 and in Supplemental Material Sec. S1). To provide additional support for (C1), we directly simulate Eq. (2) from a set of initial conditions and verify that the synchronization error e does not approach zero whenever $F^{(1)} = \cdots = F^{(N)}$, where e is defined as the standard deviation of the node state vectors, or equivalently,

$$e^2 := \frac{1}{N}\sum_{i=1}^{N}\sum_{\ell=1}^{L} ||\boldsymbol{x}_\ell^{(i)} - \overline{\boldsymbol{x}}_\ell||^2, \quad \overline{\boldsymbol{x}}_\ell := \frac{1}{N}\sum_{i=1}^{N} \boldsymbol{x}_\ell^{(i)}. \tag{D1}$$

Here $||\cdot||$ denotes the 2-norm in the state space of the subnode dynamics, and $e = 0$ is achieved if and only if the system is in a synchronous state of the form $\boldsymbol{x}_\ell^{(i)} = \boldsymbol{s}_\ell(t)$. To complete our procedure, we verify condition (C2)′, which rigorously establishes (C2).

Appendix E: Details on example in Fig. 2

In the example system from Fig. 3, the coupling matrices for the two link types are $B^{(1)} = \left(\begin{smallmatrix} b & b \\ 0 & 0 \end{smallmatrix}\right)$ and $B^{(2)} = \left(\begin{smallmatrix} 0 & 0 \\ 0 & b \end{smallmatrix}\right)$, where the constant b represents the coupling strength common to all external sublinks. The coupling matrix $F^{(i)}$ for internal sublinks is chosen from the binary set $\mathcal{F} = \{\left(\begin{smallmatrix} 0 & a \\ 0 & 0 \end{smallmatrix}\right), \left(\begin{smallmatrix} 0 & 0 \\ a & 0 \end{smallmatrix}\right)\}$, corresponding to the two possible sublink directions [and thus to two types of nodes indicated by green and cyan color, respectively, in Fig. 3(a)], where the constant a represents the coupling strength common to all internal sublinks. The Lorenz dynamics of the subnodes and the coupling represented by sublinks are given by

$$\begin{aligned} \boldsymbol{f}(\boldsymbol{x}) &= \begin{pmatrix} \gamma(x_2 - x_1) \\ x_1(\rho - x_3) - x_2 \\ x_1 x_2 - \beta x_3 \end{pmatrix}, \\ \boldsymbol{h}(\boldsymbol{x}) &= \begin{pmatrix} x_2 \\ 0 \\ 0 \end{pmatrix}, \quad \boldsymbol{x} = \begin{pmatrix} x_1 \\ x_2 \\ x_3 \end{pmatrix} \end{aligned} \tag{E1}$$

with the standard parameters, $\gamma = 10$, $\rho = 28$, and $\beta = 8/3$.

The stability function $\psi(\lambda)$ is determined by Eq. (C2), which for this system reads

$$\begin{pmatrix} \dot{\xi}_1 \\ \dot{\xi}_2 \\ \dot{\xi}_3 \end{pmatrix} = \begin{pmatrix} -\gamma & \gamma - \lambda & 0 \\ \rho - s_3 & -1 & -s_1 \\ s_2 & s_1 & -\beta \end{pmatrix} \begin{pmatrix} \xi_1 \\ \xi_2 \\ \xi_3 \end{pmatrix}, \tag{E2}$$

where $\boldsymbol{\xi} := (\xi_1, \xi_2, \xi_3)^T$ is the variation of the state vector $\boldsymbol{x}$ and the synchronous state $\boldsymbol{s} := (s_1, s_2, s_3)^T$ satisfies the equation for a single isolated Lorenz oscillator:

$$\begin{aligned} \dot{s}_1 &= \gamma(s_2 - s_1), \\ \dot{s}_2 &= s_1(\rho - s_3) - s_2, \\ \dot{s}_3 &= s_1 s_2 - \beta s_3. \end{aligned} \tag{E3}$$

For a given λ in the complex plane, we compute $\psi(\lambda)$ by numerically integrating Eqs. (E2) and (E3) for 2×10^4 time units and estimating the MLE [31] associated with the variable $\boldsymbol{\xi}$. Figure 6 shows the resulting estimate